RESEARCH ARTICLE

Controlled Growth of Hybrid Halide Perovskites by Crown Ether Complexation for Perovskite Solar Cells

Sun Ju Kim,[a] Ramesh Kumar Chitumalla,[a] Jong-Min Kim,[a] Joonkyung Jang,[a] Jin-Woo Oh,[a, b] Jovana V. Milić,*[c] and Ji-Youn Seo*[a, b, d]

[a] Department of Nano Fusion Technology, Pusan National University, 46241 Busan, Republic of Korea, e-mail: j-y.seo@pusan.ac.kr
[b] Bio-IT fusion Technology Research Center, Pusan National University, 46241 Busan, Republic of Korea
[c] Adolphe Merkle Institute, University of Fribourg, CH-1700 Fribourg, Switzerland, e-mail: jovana.milic@unifr.ch
[d] Research Center of Energy Convergence Technology, Pusan National University, 46241 Busan, Republic of Korea

Host-guest complexation has demonstrated potential for controlling hybrid organic-inorganic metal halide perovskite materials. In particular, crown ethers have been used due to their capacity to interact with metal cations (*e.g.*, Pb^{2+}) and small organic cations (*e.g.*, methylammonium (MA)), which can affect hybrid perovskite materials and their solar cells. However, this strategy has been underexploited in perovskite photovoltaics, and the underlying mechanisms are not well understood. In this study, we investigate the influence of 15-crown-5 (**15C5**) and its benzannulated derivative (benzo-15-crown-5, **B15C5**), as well as amino-functionalized analogues (15-crown-5)-2-methylamine, **2A-15C5**, and 4′-aminobenzo-15-crown-5, **4A-B15C5**, on $MAPbI_3$ perovskite crystallization and inverted solar cell performance. We demonstrate the propensity of crown ether modulators to interact with Pb^{2+} cations at the perovskite interface by density functional theory calculations. This has been shown to facilitate oriented crystal growth and homogeneous film formation, as revealed by X-ray diffraction analysis complemented by scanning electron microscopy. As a result, we demonstrate an increase in the power conversion efficiency of the solar cells of interest to advancing hybrid photovoltaics.

Keywords: ion complexation, host–guest complexation, host–guest systems, hybrid halide perovskites, perovskite solar cells.

Introduction

Perovskite solar cells (PSCs) have recently emerged as one of the leading solar cell technologies due to superior optoelectronic characteristics, stimulating efforts towards commercialization.[1–3] The photoactive layer of PSCs consists of ABX_3 metal halide perovskite materials, including the monovalent A cation (A^+), divalent metal cation (B^{2+}), and halide anion X (X^-). They form a $\{BX_6\}$ corner-sharing octahedral framework with the A cation occupying the central cavity.[2,4] Various types of metal halide perovskite materials can be used in solar cells, which mostly involve lead (Pb) and tin (Sn) as metal cations and different halide anions (X=Cl, Br, and I). A-cation can be either inorganic (such as Cs^+) or organic ammonium cation (*e.g.*, methylammonium (MA) or formamidinium (FA)). The first reported perovskite solar cell applications involved methylammonium lead iodide ($MAPbI_3$) and bromide ($MAPbBr_3$), which are archetypical perovskite materials.[1] They are applied in either normal (n-i-p) or inverted (p-i-n) PSC device architectures. Despite the advantages of their planar structure and suitability for tandem solar cells,[5–8] inverted devices have yet to be studied as much as normal PSCs. Recently, self-assembled interfacial materials, such as MeO-2PACz ([2-(3,6-dimethoxy-9*H*-carbazol-9-yl)ethyl]phosphonic acid), have attracted considerable attention as selec-

tive charge-extraction layers contributing to the increase in the efficiency of inverted PSCs (*Figure 1,a*).[5–8] However, high-quality perovskite thin films and their interfaces are still required to increase the performance and stability of PSCs, which stimulates ongoing efforts. For this purpose, compositional engineering and various treatment methods have been investigated to achieve optimal band gaps and stable photoactive perovskite structures.[2,9,10] In particular, additive engineering has been used to improve the photovoltaic performances of PSCs.[11–14] For instance, ionic salts and small organic molecules were especially relevant as interfacial modulators or spacers that form layered or two-dimensional (2D) perovskites featuring enhanced stabilities.[15–21] The use of crown ethers as interfacial modulators has recently demonstrated the capacity to increase the performance of PSCs through host-guest complexation.[22–28]

Crown ethers are known to interact with metal cations (*e.g.* Cs^+ and Pb^{2+}) as well as organic cations (*e.g.* MA or FA) through either metal coordination or hydrogen bonding,[27,28] which was found to affect perovskite crystal structure and interfacial characteristics of the corresponding films and devices.[28] However, the underlying mechanisms for their operation still need to be fully understood, and their utility across perovskite solar cell architectures, including inverted devices, remains unexploited. For instance, crown ethers in conventional triple cation double halide perovskites were suggested to promote the formation of high-quality crystals through Cs

complexation.[24,25] These studies, however, do not consider the impact of competing interactions on crystal growth, including the complexation of Pb^{2+}. Moreover, while previous reports mainly relied on non-benzannulated or dibenzo-derivatives,[23,27,28] mono-benzannulated systems still need to be investigated despite their potential to feature more directional interfacial modulation.

Here, we study representative crown ethers as modulators of archetypical MAPbI$_3$ perovskite materials and their interactions with metal ions, Pb^{2+} in particular. For this purpose, we rely on 15-crown-5 (**15C5**), benzo-15-crown-5 (**B15C5**), and their amino-functionalized derivatives, namely (15-crown-5)-2-methylamine (**2A-15C5**) and 4′-aminobenzo-15-crown-5 (**4A-B15C5**; *Figure 1,b*). We demonstrate the role of crown ether functionalization in perovskite film formation and the performance of inverted perovskite solar cells.

Results and Discussion

Crown ether modulation was investigated in inverted perovskite solar cells of p-i-n device architectures (*Figure 1,a*) employing methylammonium lead iodide (MAPbI$_3$) as archetypical perovskite material.[2,29] The film and device preparation methods are provided in the *Experimental Section* and the *Supporting Information*.

For the design of molecular modulators, the core 15-crown-5 (**15C5**) structure was selected due to its compatibility with binding Pb^{2+} ions (175 pm).[28] Moreover, benzannulated crown ether analogues were considered effective in controlling crystal growth[23] and improving contact with hole-transporting materials. In addition, analogues with amine functional groups were considered as they could contribute to the structural control through interaction with the perovskite surface by hydrogen bonding that mimics A-cation binding to the perovskite interface (*Figure 1,b*).

Density functional theory (DFT) simulations were performed to evaluate the binding of representative crown ether modulators to Pb^{2+}. They were optimized at the B3LYP/6-31G(d) level of theory using Gaussian 16 software.[30] The optimized structures were then used to evaluate the binding energies to Pb^{2+} in vacuum. We used B3LYP functional and 6-31G(d) basis set for lighter elements (H, C, N, and O) and LanL2DZ effective core potential for the heavy metal atom (Pb).[31–35] Binding energies (BE) of Pb^{2+} with crown
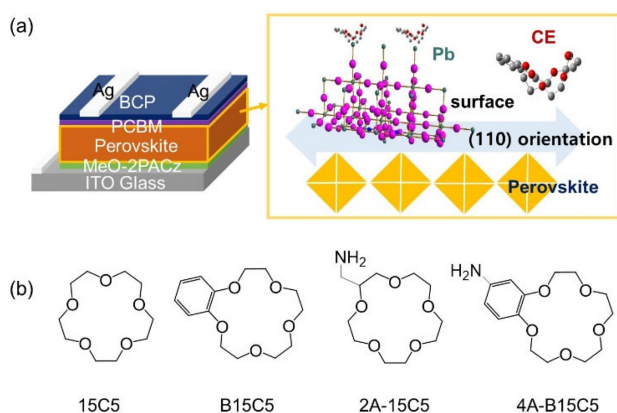

Figure 1. (a) Schematic representation of inverted perovskite solar cell architecture and the related perovskite material. (b) The structure of crown ether modulators used in this study, abbreviated as **15C5**, **B15C5**, **2A-15C5**, and **4A-B15C5**. ITO = indium doped tin oxide; MeO-2PACz = [2-(3,6-dimethoxy-9*H*-carbazol-9-yl)ethyl]phosphonic acid; BCP = bathocuproine, PCBM = phenyl-C$_{60}$-butyric acid methyl ester.

ethers (*Table 1*) were evaluated using *Eqn. 1*: and the electronic energies of crown ether, Pb^{2+}, and crown ether – Pb^{2+} complex.

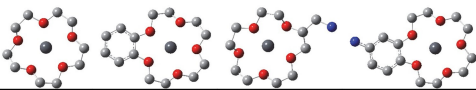$$BE = E_{CE-Pb^{2+}} - E_{CE} - E_{Pb^{2+}} \qquad (1)$$

where

$E_{CE} = $ Energy of the crown ether

$E_{Pb^{2+}} = $ Energy of Pb^{2+} ion

$E_{CE-Pb^{2+}} = $ Energy of crown ether $-Pb^{2+}$ complex.

All the *BE* values were calculated in vacuum, and a negative value of *BE* indicates stable complex formation (*Table 1*). The benzannulated crown ether modulators formed more stable complexes than the aliphatic ones (*e. g.*, $BE_{\textbf{4A-B15C5}} - BE_{\textbf{2A-15C5}} = 13.08$ kcal/mol). The DFT calculations also suggest that the additional amino functional group has the potential to stabilize the resulting host-guest complex further. These complexation effects were further investigated experimentally.

Table 1. Binding energies of crown ether modulators and Pb^{2+} in this study based on DFT calculations.

Crown ether	15C5	B15C5	2A-15C5	4A-15C5
Binding energy (kcal/mol)	−223.15	−232.00	−228.39	−241.47
Crown-ether–Pb^{2+} complexes[a]				

[a] DFT–optimized geometries at B3LYP/6-31G(d) level of theory in vacuum. The hydrogen atoms are omitted here for clarity. Gray, blue, red, and black color spheres represent C, N, O, and Pb atoms, respectively.

To assess the effect of the crown ether additives on the perovskite films, the optimized concentration of 1 mol-% of crown ethers was added to the MAPbI$_3$ precursor solutions to form a film using the anti-solvent method (experimental details are specified in the *Experimental Section* and *Figures S1 – S4* and *Tables S1 – S4*).[29,36] Films were prepared by spin coating and subsequent annealing. The structural properties and morphology of perovskite films were studied by X-ray diffraction (XRD) and scanning electron microscopy (SEM; *Figure 2*), respectively. XRD patterns evidenced the formation of a tetragonal (*I4/mcm*) MAPbI$_3$ crystal structure in accordance with the previous reports (*Figure 2,a*).[37–39] While the films processed with 1 mol-% of crown ether modulators exhibited comparable XRD patterns as the untreated reference MAPbI$_3$,[40] there was a noticeable increase in the (110)/(220) peak intensity in the treated samples, which suggests that crown ether could enhance preferential growth orientation in the (110) plane during film formation. This was more pronounced for the samples with amine-group-functionalized crown ethers (**2A-15C5** and **4A-B15C5**) than others. SEM images of the film surface (*Figure 2,b*) further indicated that the perovskite grain domains increase upon treatment with benzannulated crown ethers. The SEM cross-section, however, showed that changes in film thickness are insignificant, yet a more uniform growth was found in the **B15C5** case. In contrast, samples containing **15C5** were not uniform and featured smaller domains. This effect on the morphology suggests that the crown ether modulation could direct the formation of a more uniform perovskite film by influencing crystal growth without the appearance of a new crystal phase.

The optoelectronic characteristics were further investigated by UV-vis absorption spectroscopy and
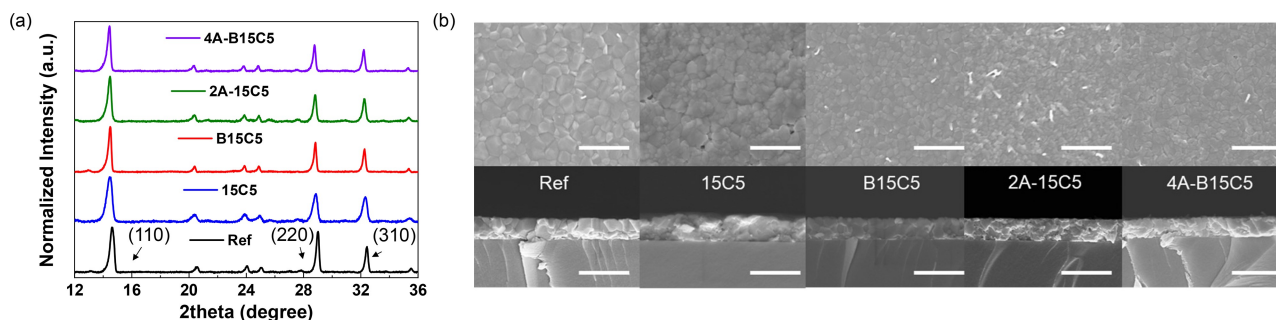

Figure 2. Structural properties and morphology of perovskite thin films prepared with and without (Ref) crown ether modulators. (a) X-ray diffraction patterns on microscope glass slides and (b) top-view (top) and cross-sectional (bottom) SEM images (scale = 1 μm) of thin films on ITO glass based on control (Ref) and treated perovskite compositions.

photoluminescence (PL) spectroscopy. UV-vis absorption spectra (*Figure 3,a*) showed a high absorption coefficient with a sharp absorption edge independently of the treatment, suggesting that the presence of modulators does not compromise optoelectronic characteristics in accordance with the XRD data. The steady-state photoluminescence (PL) measurements (*Figure 3,b*), however, indicated that PL intensity is enhanced in the treated perovskite films, except for the **4A-B15C5**, where a stronger interaction between the crown ether modulator and Pb^{2+} could result in decreasing PL.[41] In addition, the modulation resulted in a minor blue shift of the PL signals in the presence of crown ethers, which could be associated with compressive stress. These effects are relevant for the resulting photovoltaic device performances.

The effect of crown ether modulation on PSC performances was investigated in conventional indium tin oxide (ITO)/ [2-(3,6-dimethoxy-9*H*-carbazol-9-yl)ethyl]phosphonic acid (MeO-2PACz)/MAPbI$_3$/phenyl-C$_{60}$-butyric acid methyl ester (PCBM)/bathocuproine (BCP)/Ag device configuration (*Figure 1,a*).[42] The optimization identified the 1 mol-% concentration as the most effective (*Figures S1–S4, Tables S1–S4*). The photovoltaic performance (*Figure 4*) of PSCs containing **B15C5** and **2A-15C5** featured greater open-circuit voltage (V_{OC}), fill factor (FF), and power conversion efficiency (PCE) as compared to the untreated reference devices (*Table 2*). On the contrary, devices with **15C5** and **4A-B15C5** showed lower performances based on all photovoltaic parameters (*Table 2* and *Figure S5*). This is in accordance with the effect on the preferential (110)-oriented perovskite film that is favourable for efficient photovoltaic performance.[43,44] Moreover, the photovoltaic performance also corroborates the differences in the perovskite film morphology (*Figure 2,b*). The PSC devices fabricated using **B15C5** and **2A-15C5** had higher short-circuit current density (J_{SC}) as compared to control devices, which is in

Figure 4. Statistical data of photovoltaic characteristics: (a) short-circuit current density (J_{sc}), (b) open-circuit voltage (V_{oc}), (c) fill factor (FF), and (d) power conversion efficiency (PCE) collected from eight devices for the control (Ref) and modulated (**15C5**, **B15C5**, **2A-15C5**, and **4A-B15C5**) solar cells.

Table 2. Photovoltaic parameters for champion devices determined from *J–V* measurements of PSCs based on MAPbI$_3$ with different crown ether additives. The average values are obtained from the devices with statistics shown in *Figure 4*.

Devices	J_{SC} [mA/cm^2]	V_{OC} [V]	FF [%]	PCE [%]
Reference.	19.6 (19.2)	1.08 (1.06)	77.2 (67.8)	15.9 (13.8)
15C5	17.1 (16.5)	1.03 (1.00)	71.9 (62.6)	12.7 (10.3)
B15C5	19.8 (19.3)	1.10 (1.09)	79.0 (76.4)	16.5 (16.2)
2A-15C5	19.0 (18.4)	1.12 (1.11)	78.3 (76.3)	16.4 (15.6)
4A-B15C5	13.1 (12.1)	1.01 (0.99)	74.6 (67.9)	9.0 (8.1)

accordance with the incident photon-to-current conversion efficiency (IPCE) measurements (*Figure S6*). Moreover, the modulated devices featured improved open circuit voltages (V_{OC}) which point to the reduced nonradiative recombination upon modulation, corroborating with the PL analysis. The modulation, however, did not have a major effect on the current-voltage (*J–V*) hysteresis (*Figure 5*). The *J–V* curves of champion devices (*Figure 5*) corresponded to the V_{OC} of 1.09 V, J_{SC} of 18.5 mA/cm^2, FF of 76.7%, and PCE of 15.5% for control devices, whereas PSC devices treated with **B15C5** showed improvements with V_{OC} of 1.14 V, J_{SC} of 21.1 mA/cm^2, FF of 74.5%, and PCE of 18.1% (*Figure 5*). This highlights the role of crown ether modulation in photovoltaic performance.
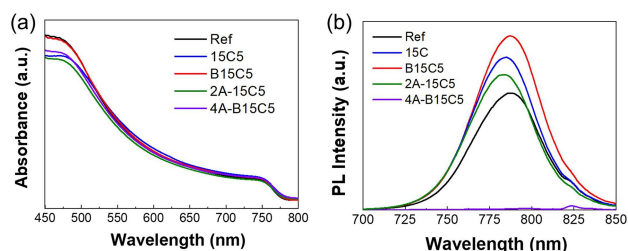

Figure 3. (a) UV-vis absorption spectra and (b) steady-state PL spectra of perovskite films before (Ref) and after modulation (**15C5**, **B15C5**, **2A-15C5**, and **4A-B15C5**).
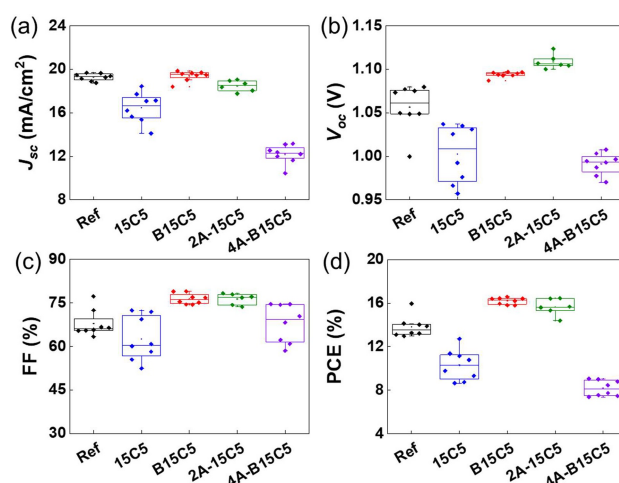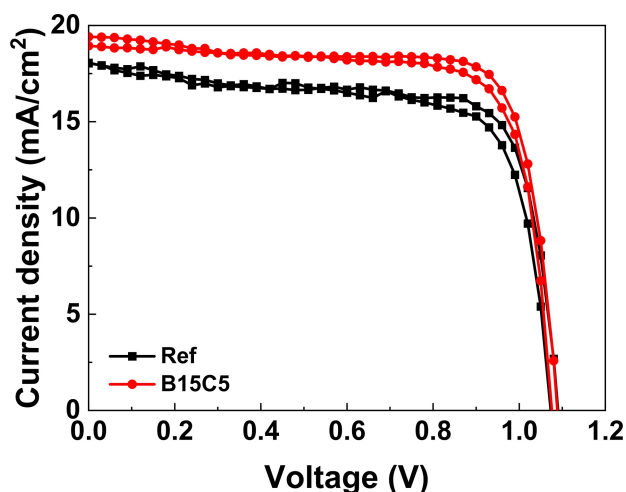
Figure 5. The *J–V* curves of the champion cells with and without crown ether modulators in reverse and forward scan direction under 1 sun (100 mW/cm^2).

Conclusions

In summary, we examined the effect of benzo- and amino-functionalized crown ethers on MAPbI$_3$ perovskite materials and inverted solar cells. We show that selected modulators have the propensity to effectively coordinate Pb^{2+} and facilitate (110)-oriented perovskite growth, as well as homogenous film formation, as evidenced by DFT calculations, XRD, and SEM. As a result, the presence of benzo-crown ethers (**B15C5**) or amino-functionalized analogues (**2A-15C5**) results in higher quality films accompanied by the average enhancement of power conversion efficiency from 15.9% to 16.5%. This suggests that either benzo- or amino-functionalization of crown ether modulators can improve the morphologies of materials and the corresponding photovoltaic characteristics, which stimulates further investigations of advanced design and application across perovskite material compositions and device architectures.

Experimental Section

Device Fabrication

Planar PSCs were fabricated in a nitrogen-filled glovebox. Indium tin oxide (ITO) glass was cleaned by ultrasonic cleaning in *Hellmanex III*, deionized water, isopropyl alcohol (IPA), and ethanol, respectively, then dried in a drying oven. Cleaned ITO glass was treated with oxygen plasma (100 W, 80 sccm, and 60 s; *COVANCE, Femto Science*, Hwaseong-si, 18469, Korea)

for 15 min before use. The hole transporting layer was prepared on ITO glass by spin-coating the [2-(3,6-dimethoxy-9*H*-carbazol-9-yl)ethyl]phosphonic acid (MeO-2PACz) (*TCI*, Japan) solution at 3000 rpm for 30 s, followed by annealing at 100 °C for 10 min on a hotplate. The perovskite precursor solution was spin-coated onto MeO-2PACz-coated substrates at 4000 rpm for 20 s. During the spin-coating process of the perovskite precursor solution (with or without the crown ether), an antisolvent treatment was performed by applying 200 μL of chlorobenzene onto the spinning substrates at 15 s before the end of the program. The substrates were immediately transferred to a hot plate and annealed at 100 °C for 20 min. To prepare the electron-transport layer, [6,6]-phenyl-C$_{61}$-butyric acid methyl ester (PC$_{60}$BM) was spin-coated onto the perovskite films at 2000 rpm for 30 s with a ramp of 1000 rpm/s followed by annealing at 100 °C for 10 min. The bathocuproine (BCP) solution was spin-coated onto the PC$_{60}$BM films at 4000 rpm for 20 s with a ramp of 2000 rpm/s followed by annealing at 70 °C for 5 min. Finally, Ag as a contact electrode was deposited by a thermal evaporator under a high vacuum (10^{-6} Torr) to a thickness of about 100 nm to complete the device.

Perovskite Film Characterization

The UV-visible absorption spectra were obtained with a UV-VIS *EVOLUTION 300*. Steady-state PL spectra were recorded using an excitation wavelength of 470 nm by an *Edinburgh FS5* spectrofluorometer. XRD patterns were collected using a *Malvern Panalytical X'Pert^3 MRD* X-ray diffractometer with a Cu radiation source. Surface and cross-sectional morphologies of the perovskite films were measured on a *Zeiss Gemini 500* field emission scanning electron microscope.

Device Characterization

Current-voltage (*J–V*) characteristics of perovskite solar cells were measured in a forward direction from −0.1 to 1.2 V using a source meter (*Keithley 4200*) under AM 1.5 illumination (100 mW cm^{-2}) from a *Sol3 A* class AAA solar simulator (*Oriel 69920*), with a step voltage of 50 mV and a delay time of 0.2 s. The light source intensity was calibrated using a standard Si solar cell. The active area defined by a metal mask aperture is 0.0435 cm^2.

Data Availability

Acknowledgments

Author Contribution Statement

The project was conceptualized by *J.-Y. S.*, who led the project, while *J. V. M.* provided inputs. The samples were prepared and characterized by *S. J. K.*, *J.-M. K.*, and *R. K. C.* under the supervision of *J.-Y. S.*, who has also written the original draft further edited by *J. V. M.*, *J. J.*, and *J.-W. O. J.-Y. S.* directed the project. All authors contributed and agreed to the final version of the manuscript.

References

[1] A. Kojima, K. Teshima, Y. Shirai, T. Miyasaka, 'Organo-metal Halide Perovskites as Visible-Light Sensitizers for Photovoltaic Cells', *J. Am. Chem. Soc.* **2009**, *131*, 6050–6051.

[2] A. K. Jena, A. Kulkarni, T. Miyasaka, 'Halide Perovskite Photovoltaics: Background, Status, and Future Prospects', *Chem. Rev.* **2019**, *119*, 3036–3103.

[3] J. Jeong, M. Kim, J. Seo, H. Lu, P. Ahlawat, A. Mishra, Y. Yang, M. A. Hope, F. T. Eickemeyer, M. Kim, Y. J. Yoon, I. W. Choi, B. P. Darwich, S. J. Choi, Y. Jo, J. H. Lee, B. Walker, S. M. Zakeeruddin, L. Emsley, U. Rothlisberger, A. Hagfeldt, D. S. Kim, M. Grätzel, J. Y. Kim, 'Pseudo-halide anion engineering for α-FAPbI₃ perovskite solar cells', *Nature* **2021**, *592*, 381–385.

[4] D. B. Mitzi, 'Templating and structural engineering in organic–inorganic perovskites', *J. Chem. Soc. Dalton Trans.* **2001**, 1–12.

[5] A. Al-Ashouri, A. Magomedov, M. Roß, M. Jošt, M. Talaikis, G. Chistiakova, T. Bertram, J. A. Márquez, E. Köhnen, E. Kasparavičius, S. Levcenco, L. Gil-Escrig, C. J. Hages, R. Schlatmann, B. Rech, T. Malinauskas, T. Unold, C. A. Kaufmann, L. Korte, G. Niaura, V. Getautis, S. Albrecht, 'Conformal monolayer contacts with lossless interfaces for perovskite single junction and monolithic tandem solar cells', *Energy Environ. Sci.* **2019**, *12*, 3356–3369.

[6] D. Song, S. Narra, M.-Y. Li, J.-S. Lin, E. W.-G. Diau, 'Interfacial Engineering with a Hole-Selective Self-As-sembled Monolayer for Tin Perovskite Solar Cells via a Two-Step Fabrication', *ACS Energy Lett.* **2021**, *6*, 4179–4186.

[7] A. Al-Ashouri, E. Köhnen, B. Li, A. Magomedov, H. Hempel, P. Caprioglio, J. A. Márquez, A. B. M. Vilches, E. Kasparavi-cius, J. A. Smith, N. Phung, D. Menzel, M. Grischek, L. Kegelmann, D. Skroblin, C. Gollwitzer, T. Malinauskas, M. Jošt, G. Matič, B. Rech, R. Schlatmann, M. Topič, L. Korte, A. Abate, B. Stannowski, D. Neher, M. Stolterfoht, T. Unold, V. Getautis, S. Albrecht, 'Monolithic perovskite/silicon tandem solar cell with >29% efficiency by enhanced hole extraction', *Science* **2020**, *370*, 1300–1309.

[8] S. Y. Kim, S. J. Cho, S. E. Byeon, X. He, H. J. Yoon, 'Self-Assembled Monolayers as Interface Engineering Nano-materials in Perovskite Solar Cells', *Adv. Energy Mater.* **2020**, *10*, 2002606.

[9] M. Saliba, T. Matsui, J.-Y. Seo, K. Domanski, J.-P. Correa-Baena, M. K. Nazeeruddin, S. M. Zakeeruddin, W. Tress, A. Abate, A. Hagfeldt, M. Grätzel, 'Cesium-containing triple cation perovskite solar cells: improved stability, reproduci-bility and high efficiency', *Energy Environ. Sci.* **2016**, *9*, 1989–1997.

[10] N. J. Jeon, J. H. Noh, W. S. Yang, Y. C. Kim, S. Ryu, J. Seo, S. I. Seok, 'Compositional engineering of perovskite materials for high-performance solar cells', *Nature* **2015**, *517*, 476–480.

[11] A. Mahapatra, D. Prochowicz, M. M. Tavakoli, S. Trivedi, P. Kumar, P. Yadav, 'A review of aspects of additive engineer-ing in perovskite solar cells', *J. Mater. Chem. A* **2020**, *8*, 27–54.

[12] S. Liu, Y. Guan, Y. Sheng, Y. Hu, Y. Rong, A. Mei, H. Han, 'A Review on Additives for Halide Perovskite Solar Cells', *Adv. Energy Mater.* **2020**, *10*, 1902492.

[13] F. Zhang, K. Zhu, 'Additive Engineering for Efficient and Stable Perovskite Solar Cells', *Adv. Energy Mater.* **2020**, *10*, 1902579.

[14] Y. Zhang, Y. Li, L. Zhang, H. Hu, Z. Tang, B. Xu, N.-G. Park, 'Propylammonium Chloride Additive for Efficient and Stable FAPbI₃ Perovskite Solar Cells', *Adv. Energy Mater.* **2021**, *11*, 2102538.

[15] J. Xi, I. Spanopoulos, K. Bang, J. Xu, H. Dong, Y. Yang, C. D. Malliakas, J. M. Hoffman, M. G. Kanatzidis, Z. Wu, 'Alter-native Organic Spacers for More Efficient Perovskite Solar Cells Containing Ruddlesden–Popper Phases', *J. Am. Chem. Soc.* **2020**, *142*, 19705–19714.

[16] M. Kim, G.-H. Kim, T. K. Lee, I. W. Choi, H. W. Choi, Y. Jo, Y. J. Yoon, J. W. Kim, J. Lee, D. Huh, H. Lee, S. K. Kwak, J. Y. Kim, D. S. Kim, 'Methylammonium Chloride Induces Intermedi-ate Phase Stabilization for Efficient Perovskite Solar Cells', *Joule* **2019**, *3*, 2179–2192.

[17] A. Ummadisingu, J.-Y. Seo, M. Stojanovic, S. M. Zakeerud-din, M. Grätzel, A. Hagfeldt, N. Vlachopoulos, M. Saliba, 'Additives, Hole Transporting Materials and Spectroscopic Methods to Characterize the Properties of Perovskite Films', *Chimia* **2017**, *71*, 754–761.

[18] J. V. Milić, J.-H. Im, D. J. Kubicki, A. Ummadisingu, J.-Y. Seo, Y. Li, M. A. Ruiz-Preciado, M. I. Dar, S. M. Zakeeruddin, L. Emsley, M. Grätzel, 'Supramolecular Engineering for For-mamidinium-Based Layered 2D Perovskite Solar Cells:

Structural Complexity and Dynamics Revealed by Solid-State NMR Spectroscopy', *Adv. Energy Mater.* **2019**, *9*, 1900284.

[19] Y. Li, J. V. Milić, A. Ummadisingu, J.-Y. Seo, J.-H. Im, H.-S. Kim, Y. Liu, M. I. Dar, S. M. Zakeeruddin, P. Wang, A. Hagfeldt, M. Grätzel, 'Bifunctional Organic Spacers for Formamidinium-Based Hybrid Dion–Jacobson Two-Dimensional Perovskite Solar Cells', *Nano Lett.* **2019**, *19*, 150–157.

[20] B. Saparov, D. B. Mitzi, 'Organic–Inorganic Perovskites: Structural Versatility for Functional Materials Design', *Chem. Rev.* **2016**, *116*, 4558–4596.

[21] G. Grancini, C. Roldán-Carmona, I. Zimmermann, E. Mosconi, X. Lee, D. Martineau, S. Narbey, F. Oswald, F. De Angelis, M. Graetzel, M. K. Nazeeruddin, 'One-Year stable perovskite solar cells by 2D/3D interface engineering', *Nat. Commun.* **2017**, *8*, 15684.

[22] T. Xiang, T. Li, M. Wang, W. Zhang, M. Ahmadi, X. Wu, T. Xu, M. Xiao, L. Xu, P. Chen, '12-Crown-4 ether assisted in-situ grown perovskite crystals for ambient stable light emitting diodes', *Nano Energy* **2022**, *95*, 107000.

[23] T.-S. Su, F. T. Eickemeyer, M. A. Hope, F. Jahanbakhshi, M. Mladenović, J. Li, Z. Zhou, A. Mishra, J.-H. Yum, D. Ren, A. Krishna, O. Ouellette, T.-C. Wei, H. Zhou, H.-H. Huang, M. D. Mensi, K. Sivula, S. M. Zakeeruddin, J. V. Milić, A. Hagfeldt, U. Rothlisberger, L. Emsley, H. Zhang, M. Grätzel, 'Crown Ether Modulation Enables over 23% Efficient Formamidinium-Based Perovskite Solar Cells', *J. Am. Chem. Soc.* **2020**, *142*, 19980–19991.

[24] R. Chen, Y. Wu, Y. Wang, R. Xu, R. He, Y. Fan, X. Huang, J. Yin, B. Wu, J. Li, N. Zheng, 'Crown Ether-Assisted Growth and Scaling Up of FACsPbI$_3$ Films for Efficient and Stable Perovskite Solar Modules', *Adv. Funct. Mater.* **2021**, *31*, 2008760.

[25] K.-W. Huang, M.-H. Li, P.-T. Hsieh, C.-F. Lin, R. Rajendran, Y.-L. Tung, P. Chen, 'Role of crown ether in the perovskite precursor for doctor-bladed perovskite solar cells: investigation by liquid-phase scanning electron microscopy', *J. Mater. Chem. C* **2022**, *10*, 16016–16027.

[26] A. Dubey, N. Kantack, N. Adhikari, K. M. Reza, S. Venkatesan, M. Kumar, D. Khatiwada, S. Darling, Q. Qiao, 'Room temperature, air crystallized perovskite film for high performance solar cells', *J. Mater. Chem. A* **2016**, *4*, 10231–10240.

[27] H. Zhang, F. T. Eickemeyer, Z. Zhou, M. Mladenović, F. Jahanbakhshi, L. Merten, A. Hinderhofer, M. A. Hope, O. Ouellette, A. Mishra, P. Ahlawat, D. Ren, T.-S. Su, A. Krishna, Z. Wang, Z. Dong, J. Guo, S. M. Zakeeruddin, F. Schreiber, A. Hagfeldt, L. Emsley, U. Rothlisberger, J. V. Milić, M. Grätzel, 'Multimodal host-guest complexation for efficient and stable perovskite photovoltaics', *Nat. Commun.* **2021**, *12*, 3383.

[28] P. Ferdowsi, U. Steiner, J. V. Milić, 'Host-guest complexation in hybrid perovskite optoelectronics', *J. Phys. Mater.* **2021**, *4*, 042011.

[29] J. Y. Seo, T. Matsui, J. Luo, J. P. Correa-Baena, F. Giordano, M. Saliba, K. Schenk, A. Ummadisingu, K. Domanski, M. Hadadian, A. Hagfeldt, S. M. Zakeeruddin, U. Steiner, M. Grätzel, A. Abate, 'Ionic Liquid Control Crystal Growth to Enhance Planar Perovskite Solar Cells Efficiency', *Adv. Energy Mater.* **2016**, *6*, 1600767.

[30] Gaussian 16, Revision C, M. J. Frisch, G. W. Trucks, H. B. Schlegel, G. E. Scuseria, M. A. Robb, J. R. Cheeseman, G. Scalmani, V. Barone, G. A. Petersson, H. Nakatsuji, X. Li, M. Caricato, A. V. Marenich, J. Bloino, B. G. Janesko, R. Gomperts, B. Mennucci, H. P. Hratchian, J. V. Ortiz, A. F. Izmaylov, J. L. Sonnenberg, D. Williams-Young, F. Ding, F. Lipparini, F. Egidi, J. Goings, B. Peng, A. Petrone, T. Henderson, D. Ranasinghe, V. G. Zakrzewski, J. Gao, N. Rega, G. Zheng, W. Liang, M. Hada, M. Ehara, K. Toyota, R. Fukuda, J. Hasegawa, M. Ishida, T. Nakajima, Y. Honda, O. Kitao, H. Nakai, T. Vreven, K. Throssell, J. A. Montgomery Jr., J. E. Peralta, F. Ogliaro, M. J. Bearpark, J. J. Heyd, E. N. Brothers, K. N. Kudin, V. N. Staroverov, T. A. Keith, R. Kobayashi, J. Normand, K. Raghavachari, A. P. Rendell, J. C. Burant, S. S. Iyengar, J. Tomasi, M. Cossi, J. M. Millam, M. Klene, C. Adamo, R. Cammi, J. W. Ochterski, R. L. Martin, K. Morokuma, O. Farkas, J. B. Foresman, D. J. Fox, Gaussian, Inc., Wallingford CT, 2016.

[31] P. J. Hay, W. R. Wadt, '*Ab initio* effective core potentials for molecular calculations. Potentials for K to Au including the outermost core orbitals', *J. Chem. Phys.* **1998**, *82*, 299.

[32] A. D. Becke, 'Density-functional thermochemistry. III. The role of exact exchange', *J. Chem. Phys.* **1998**, *98*, 5648.

[33] W. R. Wadt, P. J. Hay, '*Ab initio* effective core potentials for molecular calculations. Potentials for main group elements Na to Bi', *J. Chem. Phys.* **1998**, *82*, 284.

[34] A. D. Becke, 'Density-functional thermochemistry. IV. A new dynamical correlation functional and implications for exact-exchange mixing', *J. Chem. Phys.* **1998**, *104*, 1040.

[35] C. Lee, W. Yang, R. G. Parr, 'Development of the Colle-Salvetti correlation-energy formula into a functional of the electron density', *Phys. Rev. B* **1988**, *37*, 785.

[36] J.-Y. Seo, H.-S. Kim, S. Akin, M. Stojanovic, E. Simon, M. Fleischer, A. Hagfeldt, S. M. Zakeeruddin, M. Grätzel, 'Novel p-dopant toward highly efficient and stable perovskite solar cells', *Energy Environ. Sci.* **2018**, *11*, 2985–2992.

[37] J.-H. Im, I.-H. Jang, N. Pellet, M. Grätzel, N.-G. Park, 'Growth of CH$_3$NH$_3$PbI$_3$ cuboids with controlled size for high-efficiency perovskite solar cells', *Nat. Nanotechnol.* **2014**, *9*, 927–932.

[38] N. J. Jeon, J. H. Noh, Y. C. Kim, W. S. Yang, S. Ryu, S. I. Seok, 'Solvent engineering for high-performance inorganic–organic hybrid perovskite solar cells', *Nat. Mater.* **2014**, *13*, 897–903.

[39] M. T. Weller, O. J. Weber, P. F. Henry, A. M. Di Pumpo, T. C. Hansen, 'Complete structure and cation orientation in the perovskite photovoltaic methylammonium lead iodide between 100 and 352 K', *Chem. Commun.* **2015**, *51*, 4180–4183.

[40] B. Chen, Y. Bai, H. Tao, Q. Fu, L. Xiong, J. Weng, S. Wang, H. Zhao, Y. Han, J. Ding, 'Anisotropic Optoelectronic Properties of MAPbI$_3$ on (100), (112) and (001) Facets', *J. Electron. Mater.* **2021**, *50*, 6881–6887.

[41] Á. Golcs, P. Vezse, B. Á. Ádám, P. Huszthy, T. Tóth, 'Comparison in practical applications of crown ether sensor molecules containing an acridone or an acridine unit – a study on protonation and complex formation', *J. Inclusion Phenom. Macrocyclic Chem.* **2021**, *101*, 63–75.

[42] Y. Lin, A. Magomedov, Y. Firdaus, D. Kaltsas, A. El-Labban, H. Faber, D. R. Naphade, E. Yengel, X. Zheng, E. Yarali, N. Chaturvedi, K. Loganathan, D. Gkeka, S. H. AlShammari, O. M. Bakr, F. Laquai, L. Tsetseris, V. Getautis, T. D. Anthopoulos, '18.4 % Organic Solar Cells Using a High Ionization Energy Self-Assembled Monolayer as Hole-Extraction Interlayer', *ChemSusChem* **2021**, *14*, 3569–3578.

[43] Y. Ma, P. M. Hangoma, W. I. Park, J.-H. Lim, Y. K. Jung, J. H. Jeong, S. H. Park, K. H. Kim, 'Controlled crystal facet of MAPbI$_3$ perovskite for highly efficient and stable solar cell *via* nucleation modulation', *Nanoscale* **2019**, *11*, 170–177.

[44] R. Guo, B. Dahal, A. Thapa, Y. R. Poudel, Y. Liu, W. Li, 'Ambient processed (110) preferred MAPbI$_3$ thin films for highly efficient perovskite solar cells', *Nanoscale Adv.* **2021**, *3*, 2056–2064.